Intermittency enhancement in quantum turbulence in superfluid ^{4}He

Emil Varga*
National High Magnetic Field Laboratory, 1800 East Paul Dirac Drive, Tallahassee, Florida 32310, USA and Faculty of Mathematics and Physics, Charles University, Ke Karlovu 3, 121 16 Prague, Czech Republic

Jian Gao and Wei Guo†
National High Magnetic Field Laboratory, 1800 East Paul Dirac Drive, Tallahassee, Florida 32310, USA and Mechanical Engineering Department, Florida State University, Tallahassee, Florida 32310, USA

Ladislav Skrbek
Faculty of Mathematics and Physics, Charles University, Ke Karlovu 3, 121 16 Prague, Czech Republic

(Received 21 June 2018; published 4 September 2018)

Intermittency is a hallmark of turbulence, which exists not only in turbulent flows of classical viscous fluids but also in flows of quantum fluids such as superfluid ^{4}He. Despite the established similarity between turbulence in classical fluids and quasiclassical turbulence in superfluid ^{4}He, it has been predicted that intermittency in superfluid ^{4}He is temperature dependent and enhanced for certain temperatures, which is in striking contrasts to the nearly flow-independent intermittency in classical turbulence. Experimental verification of this theoretical prediction is challenging since it requires well-controlled generation of quantum turbulence in ^{4}He and flow measurement tools with high spatial and temporal resolution. Here we report an experimental study of quantum turbulence generated by towing a grid through a stationary sample of superfluid ^{4}He. The decaying turbulent quantum flow is probed by combining a recently developed He_2^* molecular tracer-line tagging velocimetry technique and a traditional second-sound attenuation method. We observe quasiclassical decays of turbulent kinetic energy in the normal fluid and of vortex line density in the superfluid component. For several time instants during the decay, we calculate the transverse velocity structure functions. Their scaling exponents, deduced using the extended self-similarity hypothesis, display nonmonotonic temperature-dependent intermittency enhancement, in excellent agreement with a recent theoretical and numerical study [L. Biferale *et al.*, Phys. Rev. Fluids **3**, 024605 (2018)].

DOI: 10.1103/PhysRevFluids.3.094601

I. INTRODUCTION

Intermittency in turbulent flows is a topic of extensive study in classical fluid dynamics research [1–5]. In fully developed turbulence, intermittency manifests itself as extreme velocity excursions that appear more frequently than one would expect on the basis of Gaussian statistics. Small-scale intermittency results in corrections to the energy spectrum and velocity structure functions that are nearly universal across a wide range of turbulent flows in classical fluids [6,7]. A question that has attracted increasing interest in recent years is whether this universality can be extended to quantum

*varga.emil@gmail.com
†wguo@magnet.fsu.edu

fluids such as superfluid ^{4}He whose hydrodynamic behavior is strongly affected by quantum effects and cannot be described by the Navier-Stokes equation [8–13].

Below about $T_\lambda \simeq 2.17$ K, liquid ^{4}He undergoes a second-order phase transition into a superfluid phase called He II. According to the two-fluid model [14], He II behaves as if it is composed of two interpenetrating liquids: a superfluid component and a normal-fluid component made off thermal excitations called phonons and rotons. While the normal fluid behaves classically, possessing finite viscosity and carrying the entire entropy content of He II, the superfluid component has neither entropy nor viscosity. Due to quantum restriction, vorticity in the superfluid is constrained into line singularities, each carrying a single quantum of circulation $\kappa \approx 9.97 \times 10^{-4}$ cm^2/s around its angstrom-size core [15]. The fraction ratio of the two fluids strongly depends on temperature. Above 1 K where both fluids are present, turbulence in He II (also termed quantum turbulence [16]) takes the form of a tangle of quantized vortices in the superfluid component, coexisting with more classical-like turbulent flow of the normal fluid. When the velocity fields of the two fluids are mismatched, a mutual friction force between them, arising from the scattering of thermal excitations off the cores of quantized vortices, provides an intercomponent energy transfer and additional dissipation, resulting in a modified turbulence scaling [17–21].

The general properties of quantum turbulence in He II above 1 K depend on the type of forcing. When the turbulence is generated by an applied heat current in He II, the two fluids are forced to move with opposite mean velocities (i.e., thermal counterflow) [14]. The mutual friction acts at all length scales in both fluids, which leads to strongly nonclassical behavior and decay [21–23]. On the other hand, when the turbulence is generated by methods conventionally used in classical fluid dynamics research, such as by a towed grid [24,25] or using counterrotating propellers [8], the two fluids can become strongly coupled by the mutual friction force at large scales and behave like a single-component fluid (i.e., quasiclassical turbulence), possessing some effective viscosity [20,26]. This coupling must break down at scales comparable to or smaller than the mean intervortex distance $\ell_Q = L^{-1/2}$ (where L denotes the vortex-line density, i.e., the vortex-line length per unit volume) since the flow of the superfluid component at these small scales is restricted to individual vortex lines and cannot match the velocity field of the normal fluid [27]. The quantity ℓ_Q is also known as the quantum length scale; it scales similarly to the Kolmogorov dissipation scale η of classical turbulence [28].

The similarity between quasiclassical turbulence in He II and turbulence in classical fluids has attracted a great deal of interest in both quantum and classical fluid dynamics research fields [29,30]. Extensive experimental, theoretical, and numerical work has been conducted to explore various properties of turbulence in He II (see the reviews in [18,31] and references therein). In recent years, intermittency in He II quasiclassical turbulence has become one of the central topics. Since the coupling of the two fluids at large scales and their decoupling at small scales are all controlled by the temperature-dependent mutual friction, one may naturally expect temperature-dependent turbulence statistics. Indeed, it has been predicted by Boué *et al.* [10] and Biferale *et al.* [12] that when probed at small scales, intermittency corrections to the scaling of higher-order velocity structure functions in He II quasiclassical turbulence should be enhanced in the temperature range $1.3 \lesssim T \lesssim 2.1$ K, with a maximum deviation from the Kolmogorov-Obukhov theory for classical turbulence [32] around 1.85 K. Early experiments conducted at low temperatures and close to T_λ did not find deviations from the statistics of classical turbulence [9,33,34]. A more recent experiment in a turbulent wake in He II covered a wider range of temperatures but also reported temperature-independent intermittency, similar to that in classical flows [13]. It should be noted, however, that the pressure and velocity probes used in these experiments all have sizes much larger than ℓ_Q and hence are sensitive only for the corresponding part of the turbulent cascade [12,13].

A reliable determination of intermittency in He II requires not only the generation of fully developed turbulence but also flow measurement tools with a spatial resolution comparable to ℓ_Q. In this paper we report an experimental study of quasiclassical turbulence generated by towing a grid through a stationary sample of He II. The velocity of the normal fluid is measured using

a recently developed He_2^* molecular tracer-line tagging velocimetry technique [19,35], while the vortex-line density in the superfluid component is determined using a traditional second sound attenuation method [24,36]. Our experimental results indeed demonstrate intermittency enhancement, in excellent agreement with the theory predictions [10,12].

II. EXPERIMENTAL METHOD

The experiment utilizes the Gao *et al.* He_2^* tracer-line visualization setup [35] as shown schematically in Fig. 1(a). A stainless steel channel (inner cross section of 9.5×9.5 mm^2 and length of 300 mm) is attached to a pumped helium bath whose temperature can be controlled within 0.1 mK. A mesh grid of 7×7 woven wires (about 8 mm in length and 0.41 mm in thickness) is supported inside the channel at the four corners and can be towed by a linear motor to move past our flow probes at a controlled speed up to about 65 cm/s. The grid is designed to have an open area of 54% so as to avoid producing secondary flows [37]. The flow generated in the wake of a moving grid is usually treated as a prototype of nearly homogeneous and isotropic turbulence, the simplest form of turbulence that has been extensively studied in classical fluid dynamics research [25,38–40]. The grid turbulence has also been utilized as a valuable vantage point in quantum turbulence research for assessing the similarities and differences between classical and quantum turbulent flows [24,28,41].

To probe the flow, we send high-intensity femtosecond laser pulses through the channel via a pair of slits (about 1 mm in width and 10 mm in length) cut into opposite sides of the channel along its length. These slits are covered with indium-sealed extension flanges and windows. As a consequence of femtosecond laser-field ionization [42], a thin line of He_2^* molecular tracers can be created along the beam path [35]. The initial thickness of the He_2^* tracer line is about 100 μm and its length matches the channel width. Above about 1 K, these He_2^* molecular tracers are completely entrained by the viscous normal fluid with negligible effect from the superfluid or quantized vortices [43]. A line of the molecules so created is then left to evolve for a drift time t_d of about 10–30 ms before it is visualized by laser-induced fluorescence using a separate laser sheet at

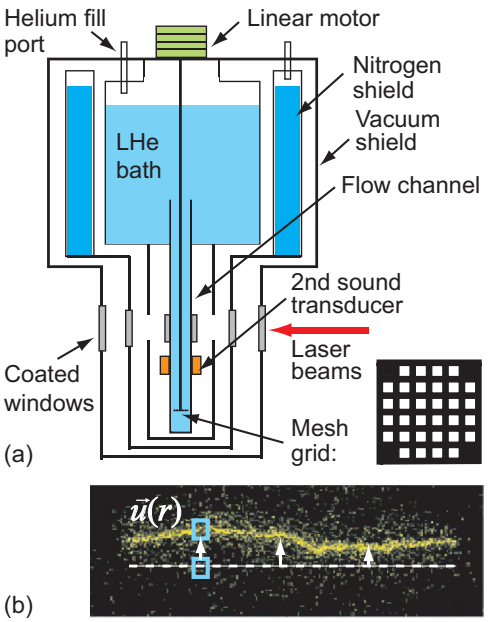

FIG. 1. (a) Schematic diagram of the experimental setup. (b) Sample image of the He_2^* molecular tracer line. The white dashed line serves to demonstrate the initial location of the trace line for velocity calculations.

905 nm for imaging [35]. The streamwise velocity $v_y(x)$ can be determined by dividing the displacement of a line segment at x by t_d [see Fig. 1(b)]. The transverse velocity increments $\delta v_y(r) = v_y(x) - v_y(x+r)$ can thus be evaluated for structure function calculations. Additionally, the flow is also probed by a standard second-sound attenuation method [35,44], revealing temporal decay of vortex-line density $L(t)$ in the superfluid.

The grid starts moving from about 50 mm below the second-sound sensors up to the uppermost position, which is roughly 100 mm above the 1×1 cm^2 visualization region. Since no steady input of energy into the flow exists (except marginal parasitic radiative heat leaks), the flow starts to decay after the passage of the grid. As the origin of time for both visualization and second-sound data, we take the instant when the grid passes the position where a tracer line would be inscribed. To study the time evolution, tracer-line inscription is delayed until the desired decay time t. The measurement at each decay time is normally repeated 100–200 times for statistical analysis, and every time the grid is towed anew. The experiments were performed in a temperature range 1.45–2.15 K with quadratically increasing decay times (typically) 1, 2, 4, and 8 s. In all cases, the grid velocity v_g was set to either 300 or 50 mm/s.

III. EXPERIMENTAL RESULTS

A. Temporal evolution of the grid turbulence

In Fig. 2 we show the profiles of the mean velocity $\overline{v_y}(x) = \langle v_y(x) \rangle_x$ and the velocity variance $\sigma(x) = \langle [v_y(x) - \overline{v_y}]^2 \rangle_x^{1/2}$ measured at 1.85 K across the channel at various decay times, where $\langle \cdots \rangle_x$ denotes an ensemble average of the results obtained at location x at each given decay time from the analysis of 100 deformed tracer-line images. Similar to typical classical grid flows, the quantum flow in the immediate wake of the grid is not perfectly homogeneous and isotropic.

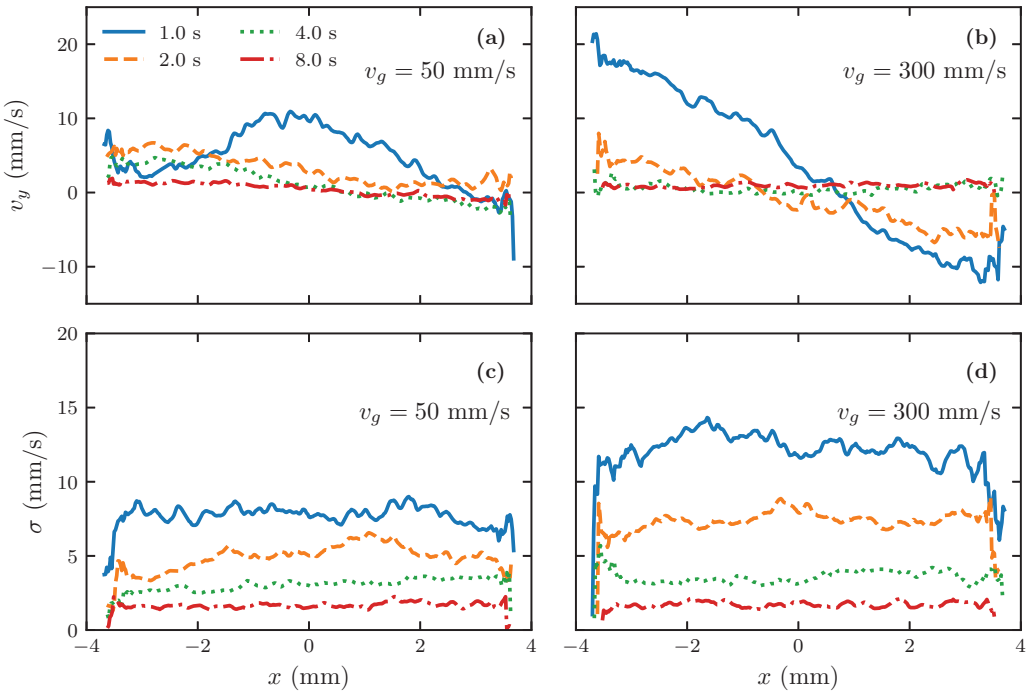

FIG. 2. (a) and (b) Ensemble-averaged velocity profile $v_y(x)$ across the channel at different decay times with grid velocities v_g as indicated. (c) and (d) Corresponding velocity variance $\sigma(x)$ profiles. The shown data are obtained at 1.85 K, at the indicated time instants.

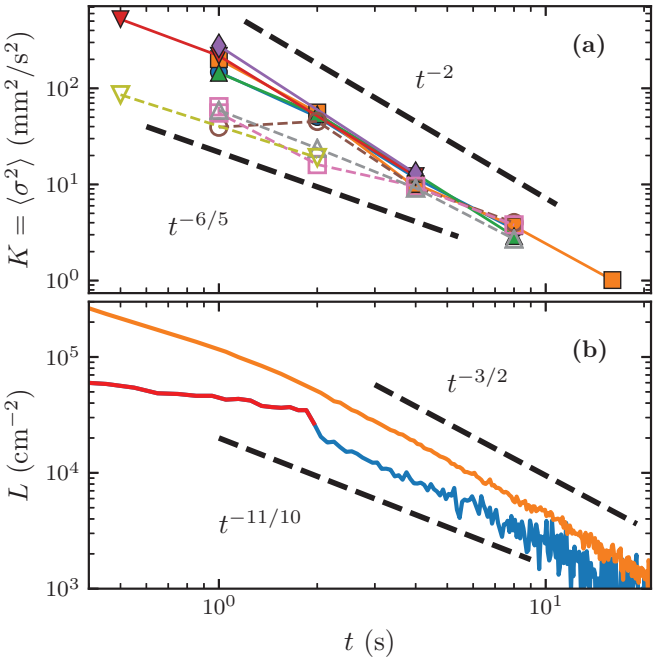

FIG. 3. (a) Decaying turbulent kinetic energy of the normal fluid $K(t)$ and (b) vortex-line density $L(t)$ originating from towing the grid at 50 mm/s (open symbols and blue line) and 300 mm/s (closed symbols and orange line). The energy decay is shown for temperatures of 1.45 K (● and ○), 1.65 K (■ and □), 1.85 K (▲ and △), 2.00 K (▼ and ▽), and 2.15 K (◆). The red line corresponds to the early decay of $L(t)$ for times when the grid is still moving. The decays are quasiclassical in character. The early part of the decay, when the energy containing length scale ℓ_e grows, displays the characteristic decay exponents $K(t) \propto t^{-6/5}$ and $L(t) \propto t^{-11/10}$, while the late universal part of the decay, when ℓ_e is saturated by the channel size, obeys $K(t) \propto t^{-2}$ and $L(t) \propto t^{-3/2}$ [24,25]. These decay rates are illustrated by thick black lines. For a towed grid velocity of 300 mm/s saturation occurs too early for the early part of the decay to be resolved. The shown data are obtained at 1.85 K.

The observed deformation of the tracer line suggests the existence of large-scale eddies spanning the entire width of the channel following the towed grid. This is most likely caused by mechanical imperfections in the construction of the grid and its support. Nevertheless, this inhomogeneity quickly decays, being virtually completely eliminated within 4 s. In contrast with the mean flow and its marked initial inhomogeneity, the profile of the velocity variance $\sigma(x)$ is much more homogeneous, even at small decay times.

Despite the initial transient inhomogeneity at large scales, seen in Fig. 2, the temporal decays of the normal fluid turbulent kinetic energy $K(t) = \langle \sigma^2 \rangle$ and the vortex-line density in the superfluid $L(t)$ exhibit clear decay characteristics of quasiclassical homogeneous isotropic turbulence, as seen in Fig. 3. As discussed in detail in Refs. [24,25], in the early decay stage of grid turbulence when the energy containing length scale ℓ_e grows from the injection scale (i.e., comparable to the mesh size) to the channel width, the characteristic decay exponents for quasiclassical homogeneous isotropic turbulence should be $K(t) \propto t^{-6/5}$ and $L(t) \propto t^{-11/10}$; in the late universal decay stage after ℓ_e is saturated by the channel width, $K(t) \propto t^{-2}$ and $L(t) \propto t^{-3/2}$ should be expected. These decay behaviors are clearly observed in our data. Note that at high towed-grid velocity (i.e., $v_g = 300$ mm/s), the saturation of ℓ_e likely occurs too rapidly for the early decay stage to be resolved. Furthermore, the transient inhomogeneity [Figs. 2(a) and 2(b)] at small decay times may also affect the decay characteristics in this regime. At the lower grid velocity (i.e., $v_g = 50$ mm/s),

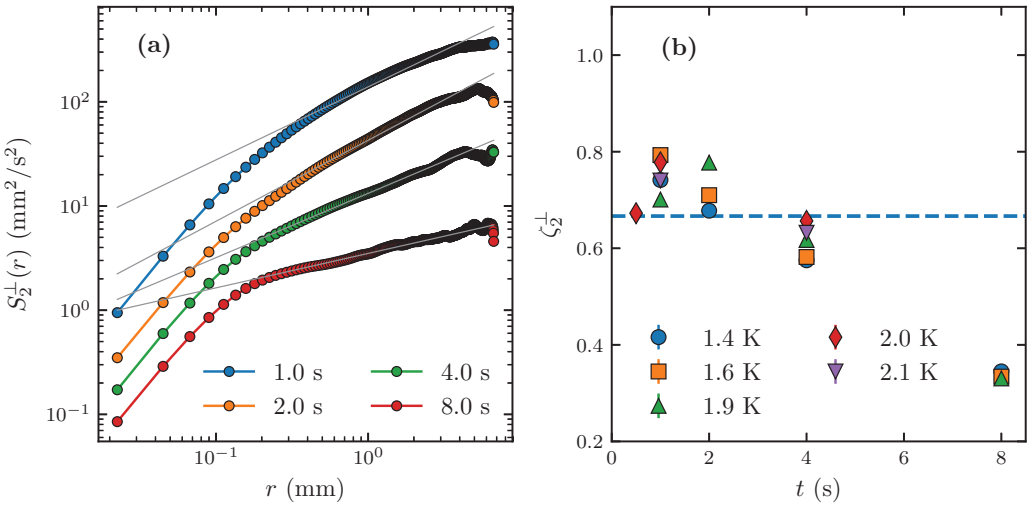

FIG. 4. (a) Calculated second-order transverse velocity structure functions $S_2^\perp(r)$ for $T = 1.85$ K at decay times indicated in the legend. The grid velocity is $v_g = 300$ mm/s. The gray solid lines represent power-law fits to the data in the range 0.2 mm $\leqslant r \leqslant$ 4 mm. (b) Scaling exponent $\zeta_2^\perp$ deduced from the power-law fits, such as that shown in (a), for temperatures shown in the legend. The dashed horizontal line shows the Kolmogorov-Obukhov scaling $\zeta_2^\perp = 2/3$.

the late universal decay stage appears at relatively large decay times (i.e., over 3–4 s) due to the slower increase of $\ell_e = \ell_e(t)$ [24,25].

B. Transverse velocity structure functions

The observed quasiclassical decay laws for $K(t)$ and $L(t)$ suggest that classical Kolmogorov-Obukhov-like scalings in other turbulence statistics such as the velocity structure functions may also be expected. For instance, for fully developed classical homogeneous isotropic turbulence, the second-order transverse velocity structure function, defined as

$$S_2^\perp(r) = \langle |v_y(x + r) - v_y(x)|^2 \rangle, \tag{1}$$

should scale with the transverse separation distance r as $S_2^\perp(r) \propto r^{2/3}$ [45].

In the case of He II grid turbulence, the situation is more complex. Figure 4(a) shows typical examples of calculated $S_2^\perp(r)$ curves, for $T = 1.85$ K with a grid velocity of $v_g = 300$ mm/s at decay times $t = 1$, 2, 4, and 8 s. Nontrivial power-law scalings of $S_2^\perp(r)$ are clearly observed in the scale range 0.2 mm $\leqslant r \leqslant$ 4 mm. The quadraticlike dependence of $S_2^\perp(r)$ at small r is probably caused by smearing of the measured velocity field limited by the width of the tracer line (i.e., about 100 μm) rather than due to the viscous flow. By fitting the data in 0.2 mm $\leqslant r \leqslant$ 4 mm with a power-law form $S_2^\perp(r) \sim r^{\zeta_2^\perp}$, the scaling exponent $\zeta_2^\perp$ can be extracted and is shown in Fig. 4(b). Data at other temperatures are also included in this figure. We see that the data display slightly steeper than Kolmogorov-Obukhov scaling (i.e., $\zeta_2^\perp > 2/3$) for the 1- and 2-s measurements and shallower than Kolmogorov-Obukhov (i.e., $\zeta_2^\perp < 2/3$) for 8-s and later measurements. We note in passing that this behavior is not unusual in classical decaying grid turbulence, especially before the wakes of individual bars of the grid fully coalesce [3,38]. An additional factor to consider is possible parasitic radiative heating to the channel. This parasitic heating can cause weak thermal counterflow, which may become important at long decay times when the grid turbulence strength is low.

Besides the second-order structure function, the Kolmogorov 4/5 law also states that within the inertial range of scales, the third-order longitudinal velocity structure function should be

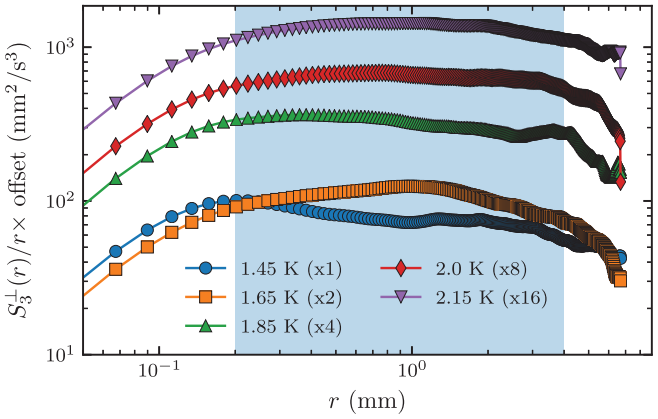

FIG. 5. Third-order transverse velocity structure functions compensated by linear scaling $S_3^\perp(r)/r$ plotted versus the separation distance r. Data for 300-mm/s grid velocity and 4-s decay time are shown for temperatures and offsets as indicated.

given by

$$S_3^\parallel(r) = -\tfrac{4}{5}\varepsilon r, \tag{2}$$

where $\varepsilon = -dK/dt$ is the energy dissipation rate [46,47]. In our experiment, only the transverse velocity structure functions $S_n^\perp$ are accessible. Nevertheless, it can be shown [46] that the scaling is equal for both $S_2^\perp$ and $S_2^\parallel$ structure functions in three-dimensional incompressible homogeneous isotropic turbulence and that the Kolmogorov 4/5 law ought to be valid also for the transverse structure function [48,49]. On the other hand, there is experimental evidence that the scaling exponent of $S_3^\perp$ in high-Reynolds-number Re atmospheric turbulence is slightly less (perhaps due to finite Re) but very close to unity [50]. We have evaluated the third-order transverse structure function $S_3^\perp(r) = \langle |v_y(x+r) - v_y(x)|^3 \rangle$ at 4-s decay time where classical scaling is clearly observed for $S_2^\perp(r)$ as shown in Fig. 4. The calculated values of $S_3^\perp(r)/r$ as a function of r are shown in Fig. 5 at various temperatures. Over a similar range 0.2 mm $\leqslant r \leqslant$ 4 mm, we see a reasonably good linear dependence of $S_3^\perp(r)$ on r, which coincides with the Kolmogorov 4/5 law in the inertial cascade range. Similar behavior is observed at 4 s for the other available temperatures and for both grid velocities; however, for decay times other than 4 s any linear scaling of $S_3^\perp(r)$ cannot be convincingly resolved.

The scaling exponents of the structure functions can also be obtained by using the so-called extended self-similarity hypothesis [51]. This hypothesis states that the scaling of a structure function $S_n(r)$ in the inertial scale range should be equivalent to the scaling of $S_n(r) \propto [S_3(r)]^{\zeta_n}$. Indeed, structure function scalings based on extended self-similarity appear to be very robust and can extend down to the dissipative scale range even for turbulent flows with moderate Reynolds numbers [52], therefore allowing for significant improvement in experimental determination of the scaling exponent ζ_n [53]. In Fig. 6(a) we show $S_2^\perp(r)$ versus $S_3^\perp(r)$ on a log-log plot for the data obtained at 1.85 K at 4-s decay time. For both grid velocities, a linear dependence of $\log S_2^\perp(r)$ on $\log S_3^\perp(r)$ is clearly seen and extends to a wide range of length scales. The values of the scaling exponent $\zeta_2^\perp$ deduced using the extended self-similarity hypothesis at various decay times and temperatures are shown in Fig. 6(b), which displays noticeably improved agreement with the Kolmogorov-Obukhov scaling.

C. Temperature dependence of intermittency corrections

Turbulence intermittency is normally evaluated by statistical analysis of the experimental data via higher-order structure functions $S_n(r)$ that are more sensitive to the occurrence of rare events.

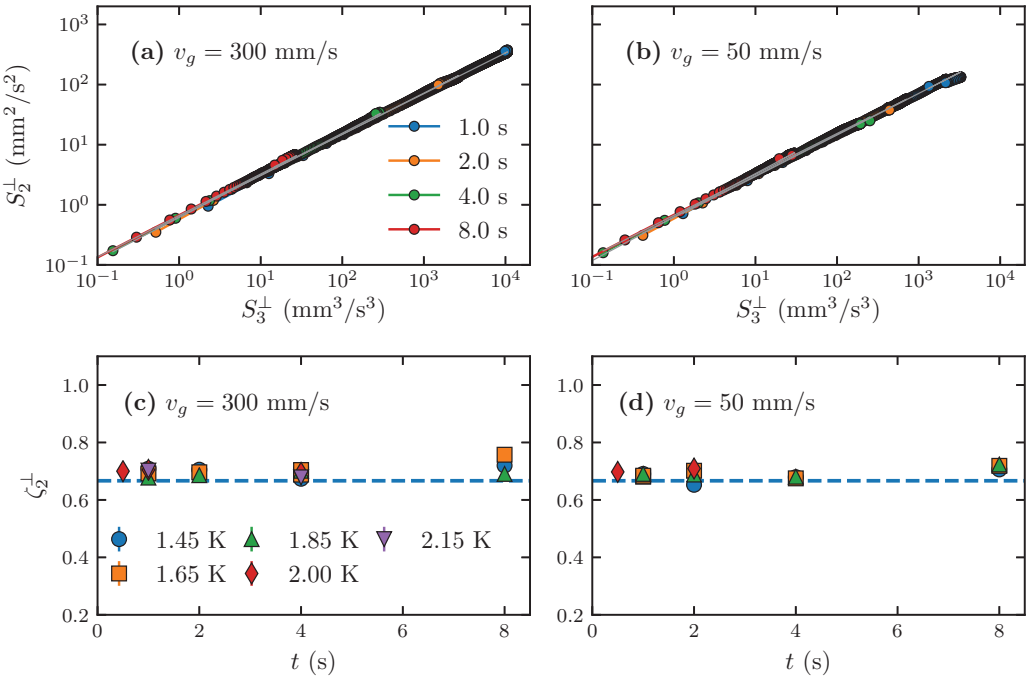

FIG. 6. (a) and (b) Extended self-similarity scaling of $S_2^\perp(S_3^\perp)$ for data obtained at $T = 1.85$ K and several decay times for the two different grid velocities, as indicated. (c) and (d) Scaling exponent $\zeta_2^\perp$ extracted using the extended self-similarity hypothesis for the two different grid velocities at a range of temperatures. The dashed horizontal lines show the Kolmogorov-Obukhov scaling $\zeta_2^\perp = 2/3$.

The transverse velocity structure function of order n is defined through the transverse velocity increments as

$$S_n^\perp(r) = \langle |\delta v_y(r)|^n \rangle = \int_{-\infty}^{\infty} dx |x|^n \, \mathrm{PDF}_r(x), \tag{3}$$

where $\mathrm{PDF}_r(x)$ represents the probability density function of $\delta v_y(r)$. In order for $S_n^\perp$ to be evaluated accurately, the experimental estimation of the PDF needs to have well-resolved tails because of the x^n term in the integral, which in turn requires very large data sets. Our setup does not presently allow for the collection of very large data sets. Typical data sets are limited to about 10^4 samples. Another issue is that, although the individual He_2^* molecules are of nanometer size and are true tracers of normal fluid flow, we cannot detect individual tracers; a large number of them closely spaced are needed to satisfy our sensitivity limit. Rare events resulting in large departures of individual tracers are therefore invisible to us. In other words, our experimentally resolved length scale is limited by the thickness of the deformed tracer line, $\ell_{\mathrm{expt}} \simeq 100$ μm. A more detailed discussion of the uncertainties associated with the calculated structure functions is provided in the Appendix.

According to the Kolmogorov-Obukhov theory, for fully developed homogeneous isotropic turbulence in classical fluids without any intermittency, the structure function in the inertial cascade range should scale as $S_n(r) \propto r^{\zeta_n}$, with the scaling exponent $\zeta_n = n/3$ [45]. Intermittency in real turbulent flows of conventional viscous fluids leads to corrections of the scaling exponents, and this correction becomes more pronounced at large n. In order to reliably determine the actual scaling exponents of the transverse structure functions $\zeta_n^\perp$ in our quantum grid turbulence, we again utilize the extended self-similarity hypothesis. Furthermore, we focus our study on data obtained at 4-s decay time, since the scalings of $S_2^\perp(r)$ and $S_3^\perp(r)$ presented in the preceding section suggest fully developed homogeneous isotropic turbulence at this decay time.

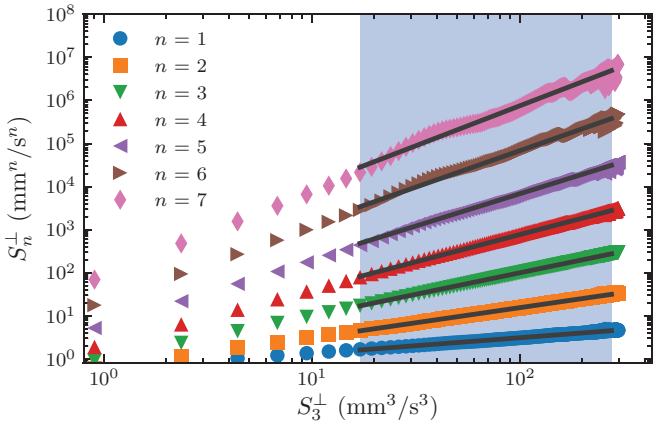

FIG. 7. Extended self-similarity. Transverse velocity structure functions $S_n^\perp$ for $n = 1$–7 are plotted versus $S_3^\perp$. The black lines are linear fits of $\log S_n^\perp$ vs $\log S_3^\perp$ to the data that fall within the shadowed region that corresponds to the shadowed region in Fig. 5 where $S_3^\perp/r$ appears to be flat. The particular case shown is for 1.85 K, 300-mm/s grid velocity, and 4-s decay time. Other cases appear qualitatively similar.

In Fig. 7, the calculated $S_n^\perp(r)$ versus $S_3^\perp(r)$ for $n = 1$–7 are shown for data obtained at 1.85 K with a grid velocity $v_g = 300$ mm/s. A clear power-law dependence of $S_n^\perp(r)$ on $S_3^\perp(r)$ is seen, which extends to the smallest scales probed in the experiment. Data obtained at other temperatures appear qualitatively similar. We then perform a power-law fit of the form $S_n^\perp(r) \propto [S_3^\perp(r)]^{\zeta_n^\perp}$ to the data (shown as black lines in Fig. 7). The fit is restricted to the range of scales 0.2 mm $< r <$ 4 mm where $S_3^\perp(r)/r$ is reasonably flat, supporting the existence of an inertial cascade.

The deduced scaling exponents $\zeta_n^\perp$, for all investigated temperatures, as a function of the order n are shown in Fig. 8. This figure represents the central result of our work. It is remarkable that the deduced scaling exponents closely follow the recent theoretical prediction of Biferale *et al.* [12], i.e., temperature-dependent intermittency corrections of the structure function scaling exponents with a maximum deviation from the Kolmogorov-Obukhov scaling at 1.85 K. It should be noted that, while the result for $t = 4$ s is robust, for small decay times (for additional discussion see the Appendix)

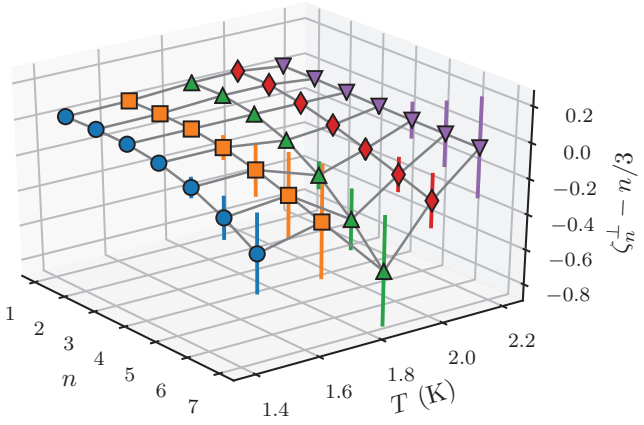

FIG. 8. Intermittency corrections to the scaling exponents of the transverse structure functions deduced through extended self-similarity for data obtained at 4-s decay time and with grid velocity $v_g = 300$ mm/s. The three-dimensional plot shows the temperature-dependent deviation of scaling exponents from Kolmogorov-Obukhov scaling: 1.45 K (●), 1.65 K (■), 1.85 K (▲), 2.00 K (◆), and 2.15 K (▼).

and for slower grid velocity the conclusion is not as clear, which is likely due to insufficiently developed turbulence.

IV. DISCUSSION

Let us compare our results with similar experimental data available. The recent measurements of Rusaouen *et al.* [13] in the wake of a disk in the two-fluid region of superfluid ^{4}He found no appreciable temperature dependence in intermittency corrections. The results of their experiment and our experiment therefore appear to be controversial. Nevertheless, there are several reasons why the two experiments may show different results. First, the prediction of temperature-dependent enhanced intermittency is explained by the authors of Refs. [10,12] via a flip-flop scenario, a random energy transfer between the normal and superfluid components due to mutual friction. While $He_2{}^*$ molecules in our experiment probe the normal fluid solely, the cantilever anemometer and pressure probes used in the Rusaouen *et al.* experiment [13] may not sense such a flip-flop exchange of energy, as it probes both fluids simultaneously. Furthermore, the sizes of the probes used in the Rusaouen *et al.* experiment are typically much larger than the quantum length scale ℓ_{Q}. Indeed, recent particle image velocimetry visualization experiments by La Mantia *et al.* [54,55], utilizing solid hydrogen or deuterium particles a few microns in size, reveal a crossover from classical to quantum signatures of turbulence as the probed length scale crosses ℓ_{Q}. As discussed previously, our smallest accessible length scale ℓ_{expt}, the width of tracer line, is about 100 μm. At a decay time of 4 s in our experiment, $\ell_{\mathrm{Q}} \simeq L^{-1/2}$ is also about 100 μm (see Fig. 3). The quantum length scale ℓ_{Q} increases at later decay times as the vortex-line density $L(t)$ decays. Therefore, our data sets sample the velocity field near or below ℓ_{Q}, where one expects the effect of quantized vorticity to become apparent. In the experiments of Rusaouen *et al.* [13], taking the outer scale of turbulence to be their channel size $\simeq$5 cm, effective kinematic viscosity $\nu_{\mathrm{eff}} \simeq 0.1\kappa$, and following the estimations in Babuin *et al.* [28], the κ-based large-scale Reynolds number at 1.85 K is roughly 6×10^4. This corresponds to $\ell_{\mathrm{Q}} \approx 7$ μm. The cantilever probe has a sensing area of 32×375 μm^2, which would translate to more than 100 quantized vortices, even if we neglect the likely increase of L in the vicinity of any obstacles [56]. The experiment of Rusaouen *et al.* [13] therefore naturally measures the same intermittency corrections as in classical turbulence.

V. CONCLUSION

We have designed and performed an experiment to study quasiclassical turbulence in the wake of a towed grid in He II, using a recently developed $He_2{}^*$ molecular tracer-line tagging velocimetry technique and a traditional second-sound attenuation method. Our main result is that, despite the fact that our data sets are not as large as they ideally ought to be, extended self-similarity reveals temperature-dependent intermittency corrections that peak in the vicinity of 1.85 K, in excellent agreement with recent theoretical predictions [10,12]. The universality of the intermittency corrections found in many different turbulent flows of classical viscous fluids [3] therefore cannot be extended to quantum turbulence in superfluid ^{4}He. It seems that the role of cliffs that are thought to be responsible for rare but intense events resulting in intermittency corrections in classical turbulence is at least partly played by quantized vortices in He II. In order to observe this "quantum" intermittency, similarly as in classical homogeneous isotropic turbulence, where one has to resolve small scales down to the Kolmogorov dissipation scale, in quantum turbulence one needs to resolve scales below the quantum length scale ℓ_{Q}.

ACKNOWLEDGMENTS

We thank V. S. L'vov, K. R. Sreenivasan, and W. F. Vinen for fruitful discussions. W.G. acknowledges support from the National Science Foundation under Grant No. DMR-1807291. The experiment was conducted at the National High Magnetic Field Laboratory, which is supported by NSF Grant No. DMR-1644779 and the state of Florida. E.V. and L.S. thank the Czech Science Foundation for support under Grant No. GAČR 17-03572S.

APPENDIX: ESTIMATION OF STRUCTURE FUNCTION ERRORS

High-order structure functions required to estimate the intermittency corrections are sensitive to rare events, events of low probability which would contribute to the tails of the statistical distribution. In samples of limited size, these tails could be underresolved, which could lead to an erroneous estimation of the structure functions. We adopt a simple strategy to estimate these errors due to lack of statistics: An estimate of the PDF is calculated from the measured data, which is then extended beyond the range of experimental data using a fit to a particular choice of a heavy-tailed statistical distribution. The difference between the values obtained through Eq. (3) using either a nonextrapolated or extrapolated PDF is then used as the estimate of the error caused by underresolved tails of the statistical distribution.

We calculate an estimation of the PDF from the measured velocity increments using the kernel density estimation (KDE) as

$$\mathrm{PDF}_r^{\mathrm{KDE}}(x) = \frac{1}{N\sqrt{2\pi}\,b}\sum_{i=0}^{N}\exp\left(-\frac{(x-\delta v_y(r)_i)^2}{2b^2}\right), \tag{A1}$$

where the sum runs through all N measured samples of $\delta v(r)_i$ at a given separation r. The result, for a particular case, is shown in Fig. 9(a). The number of samples for the 4-s decay data sets is in Fig. 10.

To estimate the error in calculating a given moment, we extrapolate the estimated PDF either by natural extension of the KDE (A1) outside the range of the data set or by using fits to either the normal (Gaussian) distribution

$$\mathrm{PDF}_r^{\mathrm{N}}(v) = \frac{1}{\sqrt{2\pi s^2}}\exp\left(-\frac{v^2}{2s^2}\right) \tag{A2}$$

or a particular case of heavy-tailed distribution

$$\mathrm{PDF}_r^{\mathrm{HT}}(v) = \frac{\exp(s^2/2)}{4m}\left[1-\mathrm{erf}\left(\frac{\log\left(\frac{|v|}{m}\right)+s^2}{\sqrt{2}s}\right)\right], \tag{A3}$$

where s and m are adjustable parameters and erf is the error function defined as $\mathrm{erf}(x) = \pi^{-1/2}\int_{-x}^{x}\exp(-u^2)du$. This form of the PDF was found to describe Lagrangian accelerations

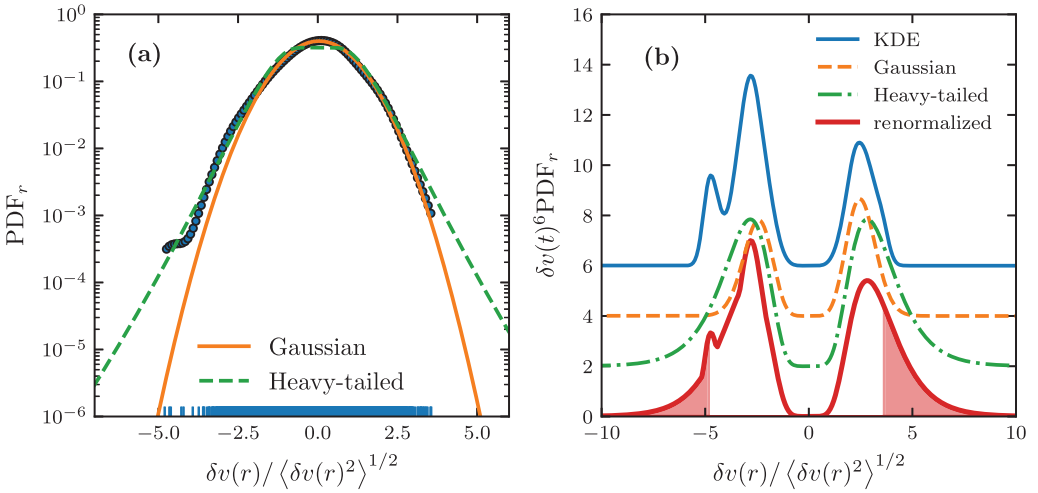

FIG. 9. (a) Probability distribution function of the velocity increments. The rug plot shows the actual data set used for the KDE. The data shown are for 1.45 K, 300-mm/s grid velocity, and 4-s decay time. (b) Calculation of the sixth moment of the velocity increment distribution. The curves are offset along the y axis with an offset incrementing by 2. The data set is the same as in (a).

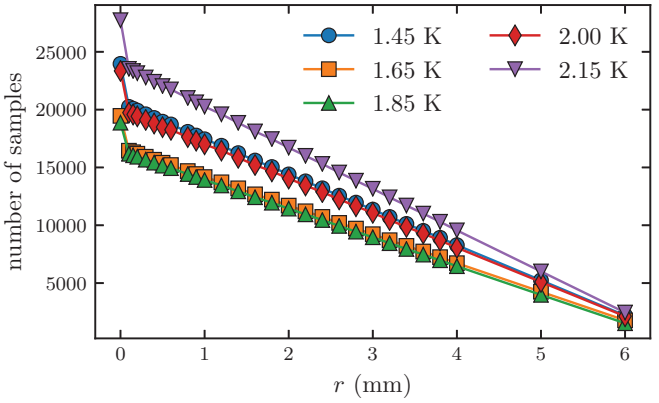

FIG. 10. Number of velocity increment samples as a function of separation for 4-s data sets and all experimental temperatures.

[57], but in our case it is used simply for reasons of convenience (we measure Eulerian transverse velocity increments), as it allows for smooth varying of the weight of the tails. Note that using a distribution with power-law tails would be inconsistent in our case as such a distribution would render the moment of sufficiently high orders undefinable. Using the two fits and the KDE, we construct a PDF with the shape of an envelope (pointwise maximum) of the three estimates. The pointwise maximum breaks the normalization of the probability density function which needs to be renormalized to the integral of unity. This effectively decreases the probability in the central peak and moves it towards the tails. An illustration of this procedure is shown in Fig. 9(b) for calculating the sixth-order moment of a distribution.

As an error estimate of the moment, we take the absolute value of the difference between the moment calculated using the natural extension of the KDE (A1) and the renormalized PDF. Graphically, this is given approximately by the area under the tails of the renormalized PDF outside the range of the data set, shown by the shaded area in Fig. 9(b). For calculation of the value of the structure function, we use $\mathrm{PDF}^{\mathrm{KDE}}$. This estimate has a very sharp cutoff (faster than normal distribution) outside the range of the experimental data set (essentially equivalent to extending a histogram with zeros) so the value is not affected by any particular choice of extrapolation. The result is shown in Fig. 11. We note that the errors of the structure functions render flatness [ratio $S_4^\perp/(S_2^\perp)^2$] unusable for quantitative analysis of intermittency.

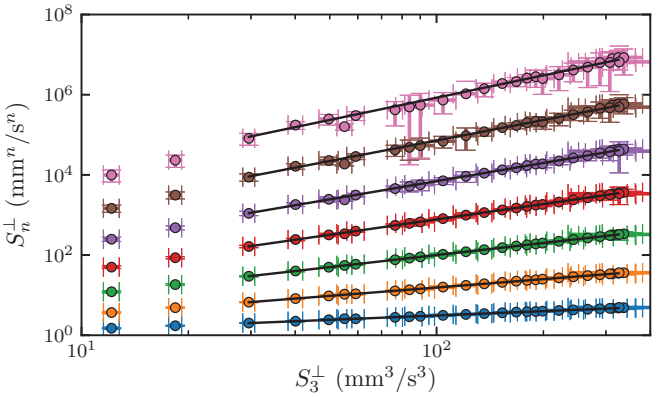

FIG. 11. Structure functions $S_n^\perp$ of orders 1–7 as a function $S_3^\perp$ at 1.85 K, 4-s decay time, and associated error bars calculated using the scheme described in the Appendix. These plots are analogs of the curves in Fig. 7.

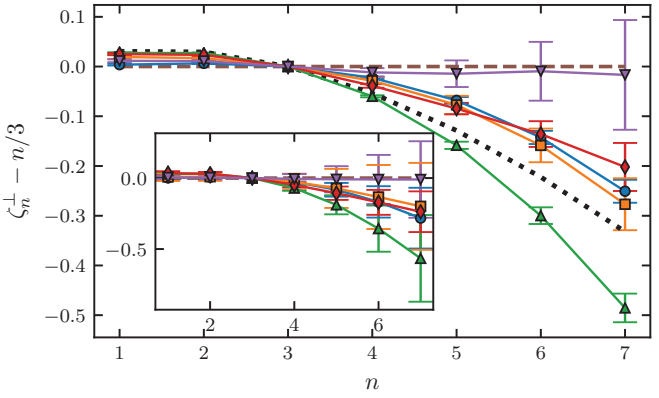

FIG. 12. Structure function scaling exponents calculated from PDF-derived structure functions. The error bars are just the standard errors of a total least-squares linear regression, also known as orthogonal distance regression. The inset shows scaling exponents of structure functions calculated using Eq. (3) (see the main text for how the error bars are calculated for the data shown in the inset). All data are for a 4-s decay time and 300-mm/s grid velocity. The temperatures are 1.45 K (●), 1.65 K (■), 1.85 K (▲), 2.00 K (◆), and 2.15 K (▼). The black dotted line shows the prediction of the She-Leveque theory [6].

We also calculate the structure functions directly from the ensemble average, using the definition (3). The intermittency corrections resulting from both procedures are shown in Fig. 12. Due to the rather arbitrary choice of the heavy-tailed distribution, the definition of the renormalized PDF, and the definition of the error itself, we also calculate the errors using a bootstrapping scheme [58]. The set of all N measured samples entering the calculation of $S_n^\perp$ in Eq. (3) is sampled at random (with possible repetitions and omissions) to form $B = 5000$ new synthetic sets of length N. The standard deviation of the moment (3) calculated for these new B data sets is used as the error. The resulting error bars are significantly smaller than those calculated using the renormalized PDF and the results are consistent with the straightforward calculation by directly averaging the sample and are not shown here.

One might justifiably become alarmed by the correlation between the number of samples in Fig. 10 and the deviation from Kolmogorov-Obukhov scaling in Fig. 12. This, however, appears to be a coincidence. The correlation is not present for other data sets, and artificially restricting the data sets at 4 s to a random choice (with replacement) of 10 000, 5000, or 2000 samples does not have a strong effect on the observed scaling exponents (although the quality of the structure functions does decrease, as is to be expected). In particular, the minimum near 1.85 K persists unaffected.

[1] A. N. Kolmogorov, A refinement of previous hypotheses concerning the local structure of turbulence in a viscous incompressible fluid at high Reynolds number, J. Fluid Mech. **13**, 82 (1962).
[2] C. Meneveau and K. R. Sreenivasan, Simple Multifractal Cascade Model for Fully Developed Turbulence, Phys. Rev. Lett. **59**, 1424 (1987).
[3] K. R. Sreenivasan and R. A. Antonia, The phenomenology of small-scale turbulence, Annu. Rev. Fluid Mech. **29**, 435 (1997).
[4] L. Biferale, Shell models of energy cascade in turbulence, Annu. Rev. Fluid Mech. **35**, 441 (2003).
[5] L. Biferale and R. Benzi, Homogeneous and isotropic turbulence: A short survey on recent developments, J. Stat. Phys. **161**, 1351 (2015).
[6] Z.-S. She and E. Leveque, Universal Scaling Laws in Fully Developed Turbulence, Phys. Rev. Lett. **72**, 336 (1994).

[7] J. Schumacher, J. D. Scheel, D. Krasnov, D. A. Donzis, V. Yakhot, and K. R. Sreenivasan, Small-scale universality in fluid turbulence, Proc. Natl. Acad. Sci. USA **111**, 10961 (2014).
[8] J. Maurer and P. Tabeling, Local investigation of superfluid turbulence, Europhys. Lett. **43**, 29 (1998).
[9] J. Salort, B. Chabaud, E. Lévêque, and P.-E. Roche, Investigation of intermittency in superfluid turbulence, J. Phys.: Conf. Ser. **318**, 042014 (2011).
[10] L. Boué, V. L'vov, A. Pomyalov, and I. Procaccia, Enhancement of Intermittency in Superfluid Turbulence, Phys. Rev. Lett. **110**, 014502 (2013).
[11] V. Shukla and R. Pandit, Multiscaling in superfluid turbulence: A shell-model study, Phys. Rev. E **94**, 043101 (2016).
[12] L. Biferale, D. Khomenko, V. L'vov, A. Pomyalov, I. Procaccia, and G. Sahoo, Turbulent statistics and intermittency enhancement in coflowing superfluid ^{4}He, Phys. Rev. Fluids **3**, 024605 (2018).
[13] E. Rusaouen, B. Chabaud, J. Salort, and P.-E. Roche, Intermittency of quantum turbulence with superfluid fractions from 0% to 96%, Phys. Fluids **29**, 105108 (2017).
[14] D. R. Tilley and J. Tilley, *Superfluidity and Superconductivity*, 3rd ed. (Institute of Physics, Bristol, 1990).
[15] R. J. Donnelly, *Quantized Vortices in Helium II* (Cambridge University Press, Cambridge, 1991).
[16] C. F. Barenghi, L. Skrbek, and K. R. Sreenivasan, Introduction to quantum turbulence, Proc. Natl. Acad. Sci. USA **111**, 4647 (2014).
[17] W. F. Vinen and J. J. Niemela, Quantum turbulence, J. Low Temp. Phys. **128**, 167 (2002).
[18] L. Skrbek and K. R. Sreenivasan, Developed quantum turbulence and its decay, Phys. Fluids **24**, 011301 (2012).
[19] A. Marakov, J. Gao, W. Guo, Steven W. Van Sciver, G. G. Ihas, D. N. McKinsey, and W. F. Vinen, Visualization of the normal-fluid turbulence in counterflowing superfluid ^{4}He, Phys. Rev. B **91**, 094503 (2015).
[20] D. Khomenko, V. S. L'vov, A. Pomyalov, and I. Procaccia, Counterflow-induced decoupling in superfluid turbulence, Phys. Rev. B **93**, 014516 (2016).
[21] J. Gao, E. Varga, W. Guo, and W. F. Vinen, Energy spectrum of thermal counterflow turbulence in superfluid helium-4, Phys. Rev. B **96**, 094511 (2017).
[22] J. Gao, W. Guo, V. S. L'vov, A. Pomyalov, L. Skrbek, E. Varga, and W. F. Vinen, Decay of counterflow turbulence in superfluid ^{4}He, JETP Lett. **103**, 648 (2016).
[23] S. Babuin, V. S. L'vov, A. Pomyalov, L. Skrbek, and E. Varga, Coexistence and interplay of quantum and classical turbulence in superfluid ^{4}He: Decay, velocity decoupling, and counterflow energy spectra, Phys. Rev. B **94**, 174504 (2016).
[24] S. R. Stalp, L. Skrbek, and R. J. Donnelly, Decay of Grid Turbulence in a Finite Channel, Phys. Rev. Lett. **82**, 4831 (1999).
[25] L. Skrbek and S. R. Stalp, On the decay of homogeneous isotropic turbulence, Phys. Fluids **12**, 1997 (2000).
[26] J. Gao, W. Guo, and W. F. Vinen, Determination of the effective kinematic viscosity for the decay of quasiclassical turbulence in superfluid ^{4}He, Phys. Rev. B **94**, 094502 (2016).
[27] J. Gao, W. Guo, S. Yui, M. Tsubota, and W. F. Vinen, Dissipation in quantum turbulence in superfluid ^{4}He above 1 K, Phys. Rev. B **97**, 184518 (2018).
[28] S. Babuin, E. Varga, L. Skrbek, E. Lévêque, and P.-E. Roche, Effective viscosity in quantum turbulence: A steady-state approach, Europhysics Lett. **106**, 24006 (2014).
[29] L. Skrbek, J. J. Niemela, and R. J. Donnelly, Turbulent flows at cryogenic temperatures: A new frontier, J. Phys.: Condens. Matter **11**, 7761 (1999).
[30] R. J. Donnelly, *High Reynolds Number Flows Using Liquid and Gaseous Helium* (Springer, New York, 1991).
[31] C. F. Barenghi, V. S. Lvov, and P.-E. Roche, Experimental, numerical, and analytical velocity spectra in turbulent quantum fluid, Proc. Natl. Acad. Sci. USA **111**, 4683 (2014).
[32] A. N. Kolmogorov, The local structure of turbulence in incompressible viscous fluid for very large Reynolds numbers, Dokl. Akad. Nauk SSSR **30**, 299 (1941) [reprinted in Proc. R. Soc. London A **434**, 9 (1991)].

[33] P.-E. Roche, C. F. Barenghi, and E. Leveque, Quantum turbulence at finite temperature: The two-fluids cascade, Europhys. Lett. **87**, 54006 (2009).
[34] J. Salort, C. Baudet, B. Castaing, B. Chabaud, F. Daviaud, T. Didelot, P. Diribarne, B. Dubrulle, Y. Gagne, F. Gauthier, A. Girard, B. Hbral, B. Rousset, P. Thibault, and P.-E. Roche, Turbulent velocity spectra in superfluid flows, Phys. Fluids **22**, 125102 (2010).
[35] J. Gao, A. Marakov, W. Guo, B. T. Pawlowski, S. W. Van Sciver, G. G. Ihas, D. N. McKinsey, and W. F. Vinen, Producing and imaging a thin line of He_2^* molecular tracers in helium-4, Rev. Sci. Instrum. **86**, 093904 (2015).
[36] W. F. Vinen, Mutual friction in a heat current in liquid helium II. II. Experiments on transient effects, Proc. R. Soc. London Ser. A **240**, 128 (1957).
[37] H. J. S. Fernando and P. D. De Silva, Note on secondary flows in oscillating-grid, mixing-box experiments, Phys. Fluids A **5**, 1849 (1993).
[38] G. Comte-Bellot and S. Corrsin, The use of a contraction to improve the isotropy of grid-generated turbulence, J. Fluid Mech. **25**, 657 (1966).
[39] H. Tennekes and J. L. Lumley, *A First Course in Turbulence* (MIT Press, Cambridge, 1972).
[40] M. Sinhuber, E. Bodenschatz, and G. P. Bewley, Decay of Turbulence at High Reynolds Numbers, Phys. Rev. Lett. **114**, 034501 (2015).
[41] S. R. Stalp, J. J. Niemela, W. F. Vinen, and R. J. Donnelly, Dissipation of grid turbulence in helium II, Phys. Fluids **14**, 1377 (2002).
[42] A. V. Benderskii, R. Zadoyan, N. Schwentner, and V. A. Apkarian, Photodynamics in superfluid helium: Femtosecond laser-induced ionization, charge recombination, and preparation of molecular Rydberg states, J. Chem. Phys. **110**, 1542 (1999).
[43] D. E. Zmeev, F. Pakpour, P. M. Walmsley, A. I. Golov, W. Guo, D. N. McKinsey, G. G. Ihas, P. V. E. McClintock, S. N. Fisher, and W. F. Vinen, Excimers He_2^* as Tracers of Quantum Turbulence in ^{4}He in the $T = 0$ Limit, Phys. Rev. Lett. **110**, 175303 (2013).
[44] S. Babuin, M. Stammeier, E. Varga, M. Rotter, and L. Skrbek, Quantum turbulence of bellows-driven ^{4}He superflow: Steady state, Phys. Rev. B **86**, 134515 (2012).
[45] J. O. Hinze, *Turbulence*, 2nd ed. (McGraw-Hill, New York, 1975).
[46] U. Frisch, *Turbulence: The Legacy of A. N. Kolmogorov* (Cambridge University Press, Cambridge, 1995).
[47] A. Noullez, G. Wallace, W. Lempert, R. B. Miles, and U. Frisch, Transverse velocity increments in turbulent flow using the RELIEF technique, J. Fluid Mech. **339**, 287 (1997).
[48] V. S. L'vov, E. Podivilov, and I. Procaccia, Exact result for the 3rd order correlations of velocity in turbulence with helicity, arXiv:chao-dyn/9705016.
[49] O. G. Chkhetiani, On the third moments in helical turbulence, JETP Lett. **63**, 808 (1996).
[50] B. Dhruva, Y. Tsuji, and K. R. Sreenivasan, Transverse structure functions in high-Reynolds-number turbulence, Phys. Rev. E **56**, R4928 (1997).
[51] R. Benzi, L. Biferale, G. Paladin, A. Vulpiani, and M. Vergassola, Multifractality in the Statistics of the Velocity Gradients in Turbulence, Phys. Rev. Lett. **67**, 2299 (1991).
[52] R. Benzi, S. Ciliberto, C. Baudet, G. Ruiz Chavarria, and R. Tripiccion, Extended self-similarity in the dissipation range of fully developed turbulence, Europhys. Lett. **24**, 275 (1993).
[53] B. Dubrulle, Intermittency in Fully Developed Turbulence: Log-Poisson Statistics and Generalized Scale Covariance, Phys. Rev. Lett. **73**, 959 (1994).
[54] M. La Mantia and L. Skrbek, Quantum, or classical turbulence? Europhys. Lett. **105**, 46002 (2014).
[55] P. Švančara and M. La Mantia, Flows of liquid ^{4}He due to oscillating grids, J. Fluid Mech. **832**, 578 (2017).
[56] P. Hrubcová, P. Švančara, and M. La Mantia, Vorticity enhancement in thermal counterflow of superfluid helium, Phys. Rev. B **97**, 064512 (2018).
[57] N. Mordant, A. M. Crawford, and E. Bodenschatz, Three-Dimensional Structure of the Lagrangian Acceleration in Turbulent Flows, Phys. Rev. Lett. **93**, 214501 (2004).
[58] B. Efron, Nonparametric estimates of standard error: The jackknife, the bootstrap and other methods, Biometrika **68**, 589 (1981).